ASME Journal of Engineering for Gas Turbines and Power
Online journal at:
https://asmedigitalcollection.asme.org/gasturbinespower

Improving the Predictive Capability of Empirical Heat Transfer Correlations for Hydrogen Internal Combustion Engines

Dominic Parsons[1]
Department of Mechanical Engineering,
University of Bath,
Claverton Down, Bath BA2 7AY, UK
e-mail: dp255@bath.ac.uk

Hao Yuan
Department of Mechanical Engineering,
University of Bath,
Claverton Down, Bath BA2 7AY, UK

Sam Akehurst
Department of Mechanical Engineering,
University of Bath,
Claverton Down, Bath BA2 7AY, UK

Stefania Esposito
Department of Mechanical Engineering,
University of Bath,
Claverton Down, Bath BA2 7AY, UK
e-mail: se662@bath.ac.uk

Hydrogen internal combustion is widely considered a viable technology to achieve near-zero tailpipe CO_2 and NOx emissions for difficult-to-electrify applications due to the maturity of ICE technology and production facilities. One-dimensional/zero-dimensional (0D) modeling is a valuable tool for engine development due to its relatively low computational requirements, but hydrogen combustion models still require further development. A large factor is gas-to-wall heat transfer, which is higher for hydrogen combustion due to higher flame temperatures and shorter quenching distance. For accurate prediction of in-cylinder temperatures, and therefore combustion rates and knock propensity, a well calibrated heat transfer model is essential. This paper evaluates existing heat transfer models against previously published experimental cylinder pressure and heat flux data from a Cooperative Fuel Research (CFR) engine with hydrogen Port Fuel Injection (PFI). A new heat transfer correlation is developed, utilizing a new fluid properties correlation to better represent the change in viscosity and conductivity with changing hydrogen concentration. Recent developments in 0D turbulence models improve the characteristic velocity calculation, which is augmented with a combustion term. This model is tested against a second dataset from the CFR engine with lambda from 1.0 to 4.0 and compression ratios of 9–13, showing improved performance versus previously published models. Whilst the new model provides more consistent results during combustion for variations in lambda and compression ratio, it requires improvement in its prediction of heat loss during expansion, and further validation at higher engine speeds and different engine configurations. [DOI: 10.1115/1.4067990]

Keywords: hydrogen, internal combustion, H2ICE, heat transfer, simulation, 0D, quasi-dimensional

1 Introduction

The transport sector is currently responsible for 22% of global CO_2 emissions, of which 41% come from passenger cars [1], making them a significant contributor toward greenhouse gas (GHG) emissions. New legislation from the EU targets zero tailpipe GHG emissions from 2035, with a goal to reach carbon neutrality in the transport sector by 2050 [2].

Hydrogen internal combustion has emerged as a promising technology to accelerate progress toward zero tailpipe GHG emissions for both on and off-highway application, with the potential for faster uptake due to the maturity of internal combustion engine technology and production capabilities.

Engine simulation forms an integral part of the development and optimization process, and gas-to-wall heat transfer is an essential element for accurate prediction of in-cylinder conditions and therefore combustion phenomena. Hydrogen combustion exhibits higher heat transfer rates than hydrocarbon combustion due to its shorter quenching distance and high flame speeds [3,4]. In 2002 Shudo et al. [5] highlighted the requirement for new heat transfer equations for hydrogen combustion for improved modeling accuracy. Despite a number of more recent studies addressing this issue [3,6], progress is still required to improve the predictive capability of zero-dimensional (0D) heat transfer models.

1.1 Heat Transfer Models. Both convective and radiative heat transfer mechanisms are present in IC engines, with radiation predominantly deriving from particulates in the combustion chamber [7–10]. SI combustion has been observed to exhibit low radiative heat transfer, reported from 3 to 10% [7,11–13], and since the only source of particulates for hydrogen combustion is trace amounts of lubricant in the crevice volume, radiation accounts for an even lower proportion of heat transfer in H_2 ICEs. This means that, conversely to diesel combustion where the contribution of radiation

The ICE Forward Conference, The Westin Riverwalk. ICEF2024.
[1]Corresponding author.
Manuscript received November 28, 2024; final manuscript received December 12, 2024; published online March 18, 2025. Editor: Jerzy T. Sawicki.

should be included [14], the radiative component can be ignored for hydrogen SI combustion.

Phenomenological heat transfer relationships applied to 0D/quasi-dimensional combustion models assume the heat transfer to be quasi-steady. This allows the convective heat transfer to be described by Eq. (1) where q is the heat flux, h is the convective heat transfer coefficient, and T_{gas} and T_{wall} are the bulk gas and wall temperatures respectively

$$q = h(T_{gas} - T_{wall}) \tag{1}$$

The Reynolds analogy (Eq. (2)), based on heat and momentum transfer in fully developed turbulent boundary layers, provides the basis for most empirical heat transfer models, with the Nusselt and Reynolds numbers described by Eqs. (3) and (4)

$$\mathrm{Nu} = a \cdot \mathrm{Re}^{b} \cdot \mathrm{Pr}^{c} \tag{2}$$

$$\mathrm{Re} = \frac{\rho \cdot v_c \cdot L_c}{\mu} \tag{3}$$

$$\mathrm{Nu} = \frac{h \cdot L_c}{k} \tag{4}$$

Since the Prandtl number (Pr) does not vary significantly during an engine cycle for most fuels, Eq. (2) is often rewritten as a function of the characteristic length L_c, characteristic velocity v_c, thermal conductivity k, dynamic viscosity μ and density ρ of the combustion gases using the definitions of the Nusselt and Reynolds numbers in Eqs. (3) and (4)

$$h = a \cdot v_c^{b} \cdot L_c^{b-1} \cdot k \cdot \mu^{-b} \cdot \rho^{b} \tag{5}$$

where a and b are model coefficients.

This equation can be further simplified into a general equation as demonstrated by Michl et al. [3]

$$h = C \cdot L_c \cdot \Omega \cdot v_c \cdot \Xi \tag{6}$$

where C denotes an overall adjustable multiplier, Ω represents the mixture properties term (equal to $k \cdot (\frac{\rho}{\mu})^{b}$), and Ξ represents the combustion term, which for some models is included in the characteristic velocity term. This is the form of a number of popular heat transfer models, most notably the highly cited Woschni model [15] which is still commonly used for ICE simulations, and has been used as a basis for the development of improved correlations for different fuels and combustion strategies [6,16–20].

Morel et al. [21] used the Colburn analogy (Eq. (7)), valid when Prandtl numbers are close to unity and the Reynolds numbers are not too far above transition, to derive a formula for the heat transfer coefficient

$$\mathrm{St} = \left(\frac{c_f}{2} \cdot \mathrm{Pr}^{-2/3}\right) \tag{7}$$

where c_f is the friction coefficient and St is the Stanton number defined by

$$\mathrm{St} = \frac{\mathrm{Nu}}{\mathrm{Re} \cdot \mathrm{Pr}} \tag{8}$$

Assuming turbulent flow over a smooth flat plate [6], the friction coefficient c_f can be approximated by

$$c_f \approx 0.0592 \cdot \mathrm{Re}^{-0.25} \tag{9}$$

Combination of Eqs. (3), (4), (7), (8), and (9) gives a general equation for the heat transfer coefficient according to the Colburn analogy

$$h = C \cdot L_c^{-0.25} \cdot c_p \cdot \mu^{0.25} \cdot (v_c \cdot \rho)^{0.75} \cdot \mathrm{Pr}^{-2/3} \tag{10}$$

This form of heat transfer correlation was also adopted by Shubert et al. to model heat transfer during diesel combustion [22], and by Nefischer et al. for hydrogen combustion, although the latter removes the Prandtl term on the basis that it does not vary significantly [6].

Heat transfer models derived by either of the Reynolds or Colburn analogies do not vary significantly from each other, as is evident by comparison of Eqs. (5) and (10). Therefore the main difference between heat transfer models lies in how the characteristic velocity, characteristic length and mixture properties are defined, and how the effect of combustion is represented.

1.2 Zonal and Dimensional Consideration in Heat Transfer Models. Historically, 0D heat transfer models have often treated the combustion chamber as a single zone, with the characteristic length and velocity represented as homogeneous values for the whole of the combustion chamber. A number of researchers have improved upon this methodology with the so-called two-zone 0D approach [23] which considers the burned and unburned zones separately. This can be also used in combination with individually defined temperatures for each surface in the combustion chamber considering the geometry and the near-wall gas dynamics [6,21,22,24]. These models are often identified as "quasi-dimensional," since they consider the three dimensions within the cylinder in a phenomenological way before condensing them into a single coefficient. Nefischer et al. [6] also comment on the effect that consideration of bulk temperatures rather than boundary layer temperatures may have on the heat transfer predictions, although they do not deem explicit consideration of the boundary layer temperature to be necessary. Boundary layer correction factors have been used previously however [24], and will be discussed in this paper.

2 Structure of Zero/Quasi-Dimensional Heat Transfer Models

For a selection of heat transfer models from the literature, a summary of the relationships corresponding to each term in Eq. (6) is provided in Table 1, with further discussion in Secs. 2.1–2.4.

2.1 Characteristic Length. Demuynck [28] describes the characteristic length as the thickness of the hydraulic boundary layer, which is similar to Morel and Keribar's definition [21], whereas Irimescu et al. [24] equate it to the size of the largest possible eddies. There does seem to be a certain level of ambiguity in the physical meaning of the characteristic length for ICEs, which has led to a number of numerical definitions being used in the literature. Woschni chose to use the cylinder bore as the characteristic length [15], and this has been adopted by a number of subsequent models that are either based on the Woschni model, or have taken influence from it. Alternative options for the characteristic length include the cube route of the volume, as proposed by Hohenberg et al. [25], and the instantaneous height of the combustion chamber ([18]). De-Cuyper et al. [29] compare the performance of these three definitions for characteristic length during the compression stroke and concluded that the cylinder bore gave the best results, although variations in its magnitude had a limited impact due to it being raised to a low power.

Irimescu et al. [24] suggest the use of the maximum diameter of the largest eddies (considering tumble motion), so this takes the form: $\min(B/2, H_c)$ where H_c is the cylinder height.

Nefischer et al. [6] endorse the strategy of using three characteristic lengths, which relate to the three elementary surfaces in the combustion chamber (liner, piston, and roof). Morel and Keribar first proposed this strategy, where they equate the characteristic length to an estimated boundary layer thickness, which is approximated as 5% of the dimension perpendicular to each surface respectively [21].

Table 1 Summary of some prominent convective heat transfer correlations in the literature

Model	Year	L_c	Ω	v_c	Ξ
Woschni [15]	1967	B^a	$p^b T^c$	$C_1\bar{S}_p + \ldots$	$\ldots + C_2 \frac{V_d Tr}{PrVr}(p - p_m)$
Hohenberg [25]	1979	V^a	$p^b T^c$	$(C_1\bar{S}_p + \ldots$	$\ldots + C_2) \cdot T^d$
Morel [21,26]	1985	$f(\text{CylGeom})$	$\rho c_p Pr^{-2/3}$	$\sqrt{v_x^2 + v_y^2 + 2k}$	–
Woschni-Huber [27]	1990	B^a	$p^b T^c$	$\max(\text{ww}, \text{wh})$	$\ldots + C_2 \frac{V_d Tr}{PrVr}(p - p_m)$
Bargende [9]	1995	V^a	$p^b T^c$	$\frac{1}{2}\sqrt{v_p^2 + \frac{8}{3}k}$	$\left(X \cdot \frac{T_b}{T_g} \cdot \frac{T_b - T_w}{T_g - T_w} + (1 - X) \cdot \frac{T_u}{T_g} \cdot \frac{T_u}{T_g} \frac{T_u - T_w}{T_g - T_w}\right)^2$
Shudo-Suzuki [17]	2002	B^a	$p^b T^c$	$\bar{S}_p + \ldots$	$\ldots + C_2 \frac{dQ}{dt} \frac{T_r}{P_r V_r}$
Chang [18]	2004	$H^{-0.2}$	$p^b T^c$	$w_c = C_1\bar{S}_p + \ldots$	$\ldots + \frac{C_2 V_d T_r}{6 \cdot p_r V_r}(p - p_m)$
Schubert [22]	2005	$f(\text{CylGeom})$	$\rho c_p Pr^{-2/3}$	$\sqrt{v_x^2 + v_y^2 + 2k}$	–
Nefischer [6]	2009	$f(\text{CylGeom})$	$\rho c_p \mu$	$\sqrt{v_x^2 + v_y^2 + 2k}$	$dk_c = C_c \left\lvert \frac{\Delta n}{n} \right\rvert dX$
Olmeda [19]	2015	B^a	$p^b T^c$	$C_1\bar{S}_p + C_2\bar{v}_g f_w + \ldots$	$\ldots + C_3 \frac{V_d Tr}{PrVr}(p - p_m)$
Michl [3]	2015	B^a	$\kappa(\frac{\rho}{\mu})^{0.77}$	$\sqrt{v_x^2 + v_y^2 + 2k}$	$X\frac{T_b}{T_w} + (1 - X)\frac{T_u}{T_w}$
Irimescu [24]	2015	$\min(H_c, B/2)$		$\sqrt{U_f^2 + \dot{u}^2 + \left(\frac{U_p}{2}\right)^2}$	$\frac{d}{dt}((1/2V_b/(\pi H_c))^{1/2}$
Choi [20]	2020	B^a	$p^b T^c$	$C_1\bar{S}_p + \ldots$	$\ldots + C_2 \frac{V_d Tr}{PrVr}(p - p_m)$

Since the characteristic length is raised to a low power for all heat transfer coefficient correlations described in the literature, approximations for it can be considered sufficient according to a number of authors [3,6]. This also means that it tends to sit lower in the priority list when considering areas of improvement for heat transfer models.

2.2 Fluid Properties. The standard Woschni model correlates the thermal diffusivity and kinematic viscosity terms from the properties of air. This has proved sufficient for the majority of hydrocarbon combustion models since the fuel effects do not significantly impact these values. Hydrogen, however, exhibits vastly different properties, which impacts the mixture properties significantly and introduces the requirement for newly calibrated correlations. For the same reason, the impact of lambda is also significantly higher for a hydrogen-air mixture.

This aspect has been addressed by Nefischer et al. [6] and Michl et al. [3] by correlating relationships for the dynamic viscosity and thermal conductivity of hydrogen, air, and the burned mixture.

2.3 Characteristic Velocity. The characteristic velocity shows the largest variation between different authors, and has arguably the largest impact on the performance of heat transfer models.

Earlier, or more simplified, models equate the characteristic velocity to the mean piston speed with some augmentation to account for combustion effects such as the method pioneered by Woschni [15]. Phenomenological models considering the gas velocity in both directions parallel to each surface, plus a turbulent kinetic energy term, were first implemented by Morel and Keribar [21] and this method has been adopted for a number of other studies on hydrogen combustion [3,6,9] following the form of Eq. (11). Demuynck et al. [30] compared this model to the Woschni model and some experimental heat flux data, finding that the consideration of fluid properties improved the accuracy of Morel's model for different fuels under motored conditions, but still did not accurately represent the heat flux observed during combustion

$$v_c = \sqrt{v_x^2 + v_y^2 + 2k} \tag{11}$$

The definitions of the velocity vectors parallel to the combustion chamber boundary, v_x and v_y, include the effects of piston motion, swirl and squish, but notably are omitting any consideration of tumble. Previous application of this model [3,6,21,22] has been performed in swirl-dominant combustion systems, so the consideration of tumble has not been critical, but will be a significant factor to consider for tumble-based combustion systems.

Olmeda et al. [19] highlighted this gap, and developed a model to capture the tumble effects in a Woschni-based heat transfer model. Their methods relied heavily on CFD-based predictions of heat transfer, which they substituted into a Woschni-based correlation. The resulting relationship was rearranged to provide the apparent error in the characteristic velocity, the formula for which was then augmented to match the heat transfer predicted via CFD.

For consideration of a phenomenological tumble model, the mean velocity at the cylinder liner would not be affected if considering bulk gas motion only, since the increase in velocity on one side of the combustion chamber would be offset by the reduction on the opposite side. The gas velocity vectors at the head and liner could be impacted significantly though.

Irimescu et al. [24] take an alternative approach to deriving the characteristic velocity, using the kinetic energy cascade model to predict mean fluid velocities, which are then augmented during combustion by the addition of kinetic energy to the working fluid due to the expansion of the burned gas. This method uses the mean gas velocity (U, derived from the mean kinetic energy), turbulent intensity (u', derived from the turbulent kinetic energy) and instantaneous piston speed (U_p) to calculate the characteristic velocity in a form similar to that of Morel and Keribar [21]

$$v_c = \sqrt{U_{b/u}^2 + u_{b/u}'^2 + \left(\frac{U_p}{2}\right)^2} \tag{12}$$

which is applied to each of the burned and unburned zones, denoted by the subscript $_{b/u}$. Equations (11) and (12) rely on a well calibrated turbulence model to accurately reflect the in-cylinder flow fields. The turbulence model employed by Michl et al. [3], Nefischer et al. [6], and Schubert et al. [22] is based on that developed by Morel in 1985 [21]. More recent developments in quasi-dimensional turbulence models by Fogla et al. [31] have been incorporated into Gamma Technologies' GT-POWER software to enable more accurate representation of the in-cylinder turbulence with engine speed and valve timing effects accounted for via a K–k–ε 0D turbulence model. This model also incorporates the effect of tumble decay on

promotion of turbulence and their results have been confirmed against CFD simulations [31–33]. Researchers from the University of Naples have also made significant recent progress in this area [32,33].

2.4 Combustion Term. Previous studies have observed enhanced heat transfer during combustion relative to motored conditions. This effect is often included in the characteristic velocity term under the assumption that combustion impacts the gas flow field near the walls, but has also been applied independently or, in some models, excluded (see Refs. [21] and [22]).

Woschni's model, which has been used extensively for gasoline SI combustion, equated the combustion effects to the difference between the measured pressure and theoretical motored pressure [15] and included them in the characteristic velocity term. This method has been expanded on by a number or researchers who have altered the coefficients from Woschni's model to better fit their data ([16,18–20,27]). Shudo-Suzuki et al. [17] took this one step further by implementing a heat release dependent term in a Woschni-based model.

Bargende [9] took a different approach in defining an independent combustion term based on the mass fraction burned (MFB) and the temperatures of the wall and the burned and unburned gases, which Michl et al. [3] emulated with a reduced term based on those same parameters.

Both Nefischer et al. [6] and Irimescu et al. [24] proposed models which consider combustion to increase the kinetic energy of the working fluid, thereby increasing the characteristic velocity. The former equates this to a molar burn fraction, and the latter to the motion caused by the expansion of the burned gases.

The different combustion terms show some variety in interpretation of where the enhancement to heat transfer stems from during combustion. Measurements of the turbulence via laser Doppler velocimetry have revealed a large increase in turbulence intensity across the flame front, but with little difference observed ahead of the flame relative to motored conditions [34].

3 Methodology

3.1 Experimental Data. Two sources of experimental data were used for analysis of heat transfer rates from spark-ignited hydrogen combustion in a PFI CFR engine.

The first of these is the experimental work of Demuynck et al. [35] in which heat flux measurements from three positions around the circumference of the top of the cylinder liner (as detailed in Fig. 1, where "P1" is the spark plug location and "P2," "P3," and "P4" are the heat flux sensor locations) were taken at a constant engine speed of 600 rpm and ensemble averaged over 35 measured cycles. This data was used to investigate each term in the heat transfer model and derive an improved correlation, and from here on will be referred to as the "calibration data."

The second source of data is the experimental work of Nguyen et al. [36] in which a CFR engine was also operated at 600 rpm for a range of compression ratios at maximum brake torque (MBT) spark

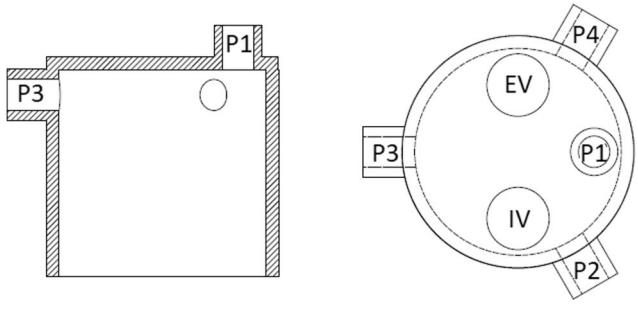

Fig. 1 Schematic of spark plug and heat flux sensor locations for Demuynck et al.'s study [35]. For this work, the measurements from the heat flux sensor at location "P2" were used.

Table 2 Engine operating conditions for the experimental data

Parameter	Cal. Data [35]	Val. Data [36]
IVO (°CA BTDC)	343	350
IVC (°CA BTDC)	154	146
EVO (°CA ATDC)	148	140
EVC (°CA BTDC)	354	345
Engine speed (rpm)	600	600
Compression ratio	8.5, 9, 9.5	9, 11, 13
Lambda	1.4–2.2	1.0–4.0
IMEP (bar)	1.5–5.8	1.6–5
Fired cases	15	26
Motored cases	5	—
Spark location	P1 (Fig. 1)	P3 (Fig. 1)
Heat flux location	P2 (Fig. 1)	—

timing for 300 cycle samples. Heat flux data were not available for this engine so performance of the heat transfer models was inferred through analysis of the measured pressure traces. These data were used to test the newly developed heat transfer model against a "blind" dataset, and from here on will be referred to as the "validation data." The engine operating conditions are detailed in Table 2.

Both experiments used bottled hydrogen supplies which were regulated down to 6 bar before injection to the intake port. Mass flow meters were installed to monitor the hydrogen flowrate.

The three measurement locations in Demuynck et al.'s study do not provide sufficient information to calculate a spatially averaged heat flux value, and the side-mounted spark plug presents an asymmetric heat flux pattern around the cylinder liner during flame propagation. After analysis of the heat flux measurements against each other, they assume that the measurement at the "P2" location is representative for the entire cylinder surface [35]. This measurement location has also been used for this study, but with the concession that a simulated spatially averaged value may not be expected to follow exact trends of the measured data.

3.2 Simulation Model. The engine models were prepared in the one-dimensional simulation platform GT-POWER, from Gamma Technologies, with a three-pressure analysis (TPA) to analyze the engine breathing and heat release rate based on measured dynamic port and in-cylinder pressures. Each TPA model was validated against the measured pressure, emissions, and flow data with the default (Woschni) heat transfer model before commencing the heat transfer investigation.

Since the calculated heat release rate is strongly dependent on the heat transfer rate, the TPA approach was used to compare the modifications to the heat transfer correlations. Simulated and experimental pressure traces were used to calibrate the heat transfer multipliers for each model, and the resulting simulated heat flux was compared to the measured heat flux data.

The engine structure temperature solver in GT-POWER is represented by a number of zones around the liner, head and piston, with basic calculations performed to predict the solid temperatures in each zone. This allows for nonuniform temperatures around the combustion chamber surfaces to be accounted for without excessive computational cost. For this study, GT-POWER's inbuilt wall solver was used to calculate cycle averaged wall temperatures for the combustion chamber. The measured temperatures had an amplitude of 5 K, so a constant temperature for each zone was considered sufficient, relative to the magnitude of the gas temperatures during combustion (up to 2000 K). The simulated temperature at the location of the heat flux sensor had a mean error of 3 K and a maximum error of 7 K versus the calibration dataset, which is within the error margin of 14 K quoted by Demuynck et al. for the measurements [35].

The modeling of a measurement node at the top of the liner to correspond to the position of the sensor may have offered an improved comparison to the measured heat flux, although any error present in the flame geometry model would likely affect the

Table 3 Table of Heat transfer multipliers calibrated for motored and fired conditions

Model	Motored	Fired	%Δ
Woschni [15]	2.1	3.2	57
Morel [21]	1.5	2.0	33
Michl [3]	0.03	0.04	33

simulated heat flux result far more than error in the heat transfer model itself. Therefore, average heat flux values and pressure measurements were used to compare to the experiments.

A zonal heat transfer model was employed, which calculates the heat transfer for the burned and unburned zones, respectively, according to the temperatures in each zone and the wall-wetting ratio for each combustion chamber surface.

3.3 Calibration of Existing Heat Transfer Models. The Woschni heat transfer model is often used as a baseline for the development of 0D heat transfer models. Whilst it is included in the following results, more recent models are presented as an alternative baseline with more evidence in the literature for their applicability to hydrogen combustion.

The models presented in this section are the Woschni model [15], Morel and Keribar's model [21], and the Michl model [3].

For each heat transfer model, the heat transfer multiplier was tuned to give the best match to the measured pressure during the compression stroke for all motored and all fired cases, respectively, with the resulting values shown in Table 3. The turbulence model of Fogla et al. [31] was implemented to provide estimates for in-cylinder gas motion, calibrated against cold-flow computational fluid dynamics (CFD) results for the motored cases.

The performance of each heat transfer model was evaluated against the measured pressure and heat flux data, which is presented in Sec. 5.

4 Development of a New Heat Transfer Coefficient Correlation

The following sections describe the development approach for each term in the convective heat transfer correlation. The simplified model structure described by Eq. (6) provides a clear framework to analyze each component of the model in detail. Rearranging the Colburn analogy into this form introduces a Prandtl term with an exponent of $1/3$, which can be included in the mixture properties term, effectively rearranging Morel's heat transfer equation into the form of Eq. (6).

A zonal approach was taken for the calculation of the heat transfer coefficient, resulting in a burned and unburned coefficient according to the mixture properties and gas dynamics adjacent to each of the elementary surfaces within each zone, respectively.

The initial focus on the compression stroke of the motored and fired data included adjustment of the exponents in the Reynolds analogy. Previous studies have reported values from 0.75 up to 0.8 for the b exponent in Eq. (5). Analysis with the available data revealed that a value of 0.75 provided the best fit during compression for both motored and fired conditions with the new mixture properties correlations detailed below implemented.

Once the unfired part of the cycle was calibrated, the focus moved onto the combustion term and selection of an appropriate relationship to improve the model's performance during combustion.

4.1 Mixture Properties. Previous updates to the mixture properties term have produced relationships for the fuel, air, and burned gases [3,6]. This study has produced new relationships for each of the major species present during hydrogen combustion to accommodate larger ranges of equivalence ratio.

The mechanism published by Sun et al. [37] was selected to investigate the gas properties with the open-source 0D software Cantera. A power law fit was found to be sufficient for each individual species for both thermal conductivity and dynamic viscosity for temperatures from 280 to 2200 K.

4.1.1 Conductivity Correlation. Four new correlations were derived from the calculated conductivity results, for each of the main species present during hydrogen combustion:

$$\kappa_{H_2} = 0.0006424 \times T^{0.9147} + 0.07337 \tag{13}$$

$$\kappa_{H_2O} = 1.771 \times 10^{-5} \times T^{1.273} \tag{14}$$

$$\kappa_{N_2} = 0.0002524 \times T^{0.8114} \tag{15}$$

$$\kappa_{O_2} = 0.0002607 \times T^{0.8158} \tag{16}$$

A comparison of these correlations is compared to those of Michl et al. [3] in Fig. 12 in Appendix B.

4.1.2 Viscosity Correlation. The calculated viscosities matched the correlations provided by Michl et al. [3] closely, with the only deviation being for the burned mixture. Nevertheless, four new correlations were produced to conform to the species-specific format used for this model

$$\mu_{H2} = 2.179 \times 10^{-7} \times T^{0.6518} \tag{17}$$

$$\mu_{H_2O} = 2.632 \times 10^{-8} \times T^{1.041} + 9.247 \times 10^{-7} \tag{18}$$

$$\mu_{N_2} = 3.03 \times 10^{-7} \times T^{0.705} + 1.839 \times 10^{-6} \tag{19}$$

$$\mu_{O_2} = 3.209 \times 10^{-7} \times T^{0.7164} + 2.431 \times 10^{-6} \tag{20}$$

A comparison of these correlations is compared to those of Michl et al. [3] in Fig. 13 in Appendix B.

4.2 Characteristic Length. Since the only engine build geometry that varied in this dataset was the compression ratio, an exhaustive analysis of the characteristic length could not be performed. It was decided to use the quasi-dimensional approach endorsed by Morel and Keribar [21] and Nefischer et al. [6] which uses the perpendicular distance from each surface. This choice was made to accommodate the difference between flow conditions adjacent to each surface within the combustion chamber. Due to the simplicity of the combustion chamber geometry in the CFR engine (no piston cup or pent roof), the calculation for the characteristic length for each surface was relatively straightforward.

4.3 Characteristic Velocity. Use of the regional velocity vector and turbulent kinetic energy (TKE) approach pioneered by Morel and Keribar [21] (Eq. (11)) requires accurate calibration of a 0D turbulence model. The k–ε turbulence model presented by Morel and Keribar [21] was adopted by Nefischer et al. [6] and Michl et al. [3] for their heat transfer correlations [3,6]. However, advances in 0D turbulence models since their publication allow further improvement in this area. The model published by Fogla et al. [31] combines k–ε and K–k approaches via three differential equations:

$$\frac{d(mK)}{dt} = C_{\text{in}} \cdot (1 - \alpha_{\text{in}}) \cdot E_{\text{in}} + K \cdot \dot{m}_{\text{out}} - P_k \tag{21}$$

$$\frac{d(mk)}{dt} = C_{\text{in}} \cdot \alpha_{\text{in}} \cdot E_{\text{in}} + k \cdot \dot{m}_{\text{out}} + P_k + C_{\text{tumb}} \cdot T - m \cdot \varepsilon \tag{22}$$

$$\frac{d(m\varepsilon)}{dt} = C_{\text{in}} \cdot E_{\text{in}} \cdot \frac{\sqrt{k}}{L_g} + \varepsilon \cdot \dot{m}_{\text{out}} - P_\varepsilon + C_{\text{tumb}} \cdot T \cdot \frac{\sqrt{k}}{L_g} - 1.92 \cdot \frac{m\varepsilon^2}{k} \tag{23}$$

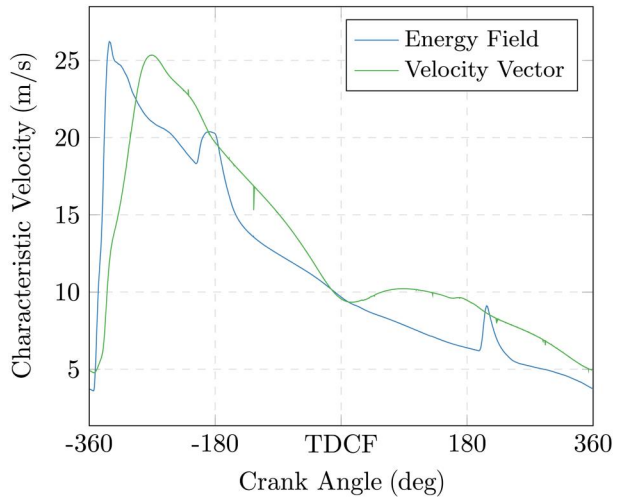

Fig. 2 A comparison between the characteristic velocity derived by Morel and Keribar's method (velocity vector) [21], and Irimescu et al.'s method (energy field) [24], for a motored condition (CR = 8.67, P_{in} = 0.99 bar)

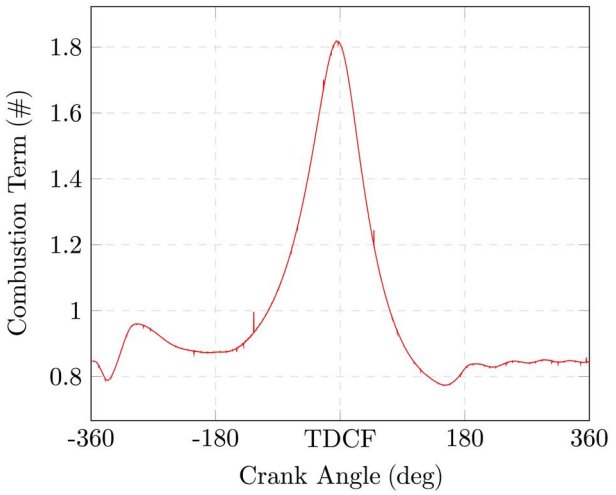

Fig. 3 The value of the combustion term of Michl et al. for a motored condition (CR = 8.67, P_{in} = 0.99 bar)

where K and k are the mean and turbulent kinetic energy and ε is the turbulent dissipation rate. This method eliminates the requirement for an arbitrarily imposed decay term for conversion of mean energy from intake flow to turbulence, which is characteristic of k–ε models. Further details of this turbulence model can be found in [31] and in Appendix A.

4.3.1 Turbulence Model Calibration. The turbulence model was calibrated against cold-flow CFD results, which provide a benchmark for the in-flow and piston motion contributions to the turbulence field in the combustion chamber. Simcenter STAR CCM+ was used to perform this analysis, using a RNG k–ε turbulence model for each of the five measured motored conditions in the calibration dataset (compression ratio from 7.7 to 9.2, throttle position from 75% to wide open throttle (WOT)). Once the turbulence model was calibrated for the motored data, the resulting model was applied to the fired data.

4.3.2 Kinetic Energy-Derived Characteristic Velocity Calculation. The approach from Irimescu et al. for deriving the characteristic velocity, described by Eq. (12), relies heavily on the flow prediction in the cylinder. A comparison performed for a motored condition on the CFR engine reveals very similar values for the characteristic velocity derived by each method, as shown in Fig. 2.

Considering the similarity in the output derived from each method, the velocity vector method has been chosen as it allows for consideration of each elementary surface independently. It should be noted that the characteristic velocity method of Irimescu et al. does include a combustion term which has not been included for this comparison, this will be discussed in Sec. 4.4.

4.4 Combustion Term. As discussed in Sec. 3.3, Morel's model, which has no combustion term, appears to underestimate the heat flux during combustion. Michl's model does have a combustion term, but it appears to overcompensate for the combustion effects on heat transfer.

Unlike a number of other models, Michl et al.'s combustion term is independent of the characteristic velocity, instead relating an increase in heat transfer to the process temperatures [3]. This takes a very similar form to the boundary layer correction term employed by Irimescu et al. [24] and does in fact impact the heat transfer during the whole cycle, rather than just during combustion.

Figure 3 illustrates the magnitude of the combustion term during a motored test, revealing an enhancement of the heat transfer coefficient of almost double at TDC due to the temperature difference between the gas and walls.

Examination of the measured heat flux shows a very steep gradient both before and after the peak, this is in part due to the single measurement location, but is also a widely reported characteristic of hydrogen combustion [3,5,6,35]. The steep rise and fall of the heat flux indicates that a combustion term is required to enhance the heat transfer during the combustion phase, but not further into the expansion phase. Further analysis of the simulated and measured heat flux traces is continued in Sec. 5.1 and illustrated in Fig. 8.

Figure 4 compares the gradients and phasing of some normalized combustion terms for a representative fired condition, along with a heat transfer coefficient calculated from the measured heat flux. The combustion terms included are those of Woschni, Michl, Nefischer, Irimescu, and Shudo-Suzuki. It is apparent that both Michl and Woschni's combustion terms prevent the fast decay indicated by the measured data. Nefischer and Shudo-Suzuki's combustion terms are similar, both being derived from the heat release rate, but the decay on the former is slightly earlier and so has been selected for this model. Nefischer also claims that the adaptation to a molar-specific burn rate improves application of the heat transfer model to methane and gasoline as well as hydrogen [6].

4.5 Boundary Layer Consideration. Irimescu et al. discovered an improvement in their heat transfer model by including a

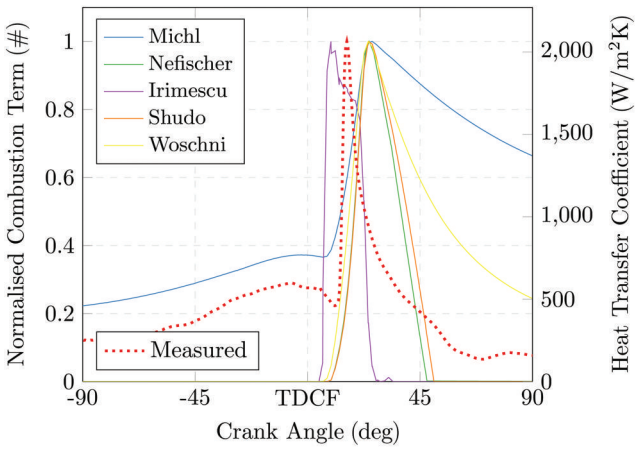

Fig. 4 Comparison of normalized combustion terms for a single operating condition (CR = 9, IMEP = 3 bar and lambda = 1.8), with the heat transfer coefficient calculated from the measured heat flux plotted against the secondary *y* axis for reference

boundary layer correction term which relates the gas to wall temperatures for the burned and unburned zones [24]

$$\left(\frac{T_{u/b}}{T_w}\right). \tag{24}$$

Michl et al.'s combustion model takes a very similar form to this, with a cumulative burn rate used to satisfy the ratio between the burned and unburned zones. The current data revealed a divergence from the measured data during the compression stroke when a temperature-dependent term was included in the heat transfer model, so it was excluded from the final formulation.

4.6 Final Model Structure. The new model takes the form shown in Eq. 25, with h calculated for the burned and unburned zones independently as discussed in Sec. 4:

$$h = \underbrace{f\,(\text{CylGeom})^{0.25}}_{L_c} \cdot \underbrace{\kappa \left(\frac{\rho}{\mu}\right)^{0.75}}_{\Omega} \cdot \underbrace{\sqrt{v_x^2 + v_y^2 + 2(k + dk_c)}^{0.75}}_{v_c \,\&\, \Xi} \cdot \text{Pr}^{1/3} \tag{25}$$

where

$$dk_c = C_{\text{comb}} \cdot \left|\frac{\Delta n}{n_{\text{init}}}\right| \cdot \frac{dQ}{m_{\text{fuel}} \cdot \text{LHV}_{\text{fuel}}} \tag{26}$$

with Δn and n_{init} representing the change in number of moles, and initial number of moles, respectively.

5 Results for the New Model Compared to the Current State of the Art

5.1 Calibration Dataset. Figures 5–8 show the cylinder pressure and heat flux calculated by each heat transfer model against the measured cylinder pressure and heat flux for representative motored and fired conditions from the calibration dataset.

The modeled heat flux traces in Fig. 6 all exhibit higher peaks than the measured data which, due to the well matched pressure traces shown in Fig. 5, provide further evidence that the single

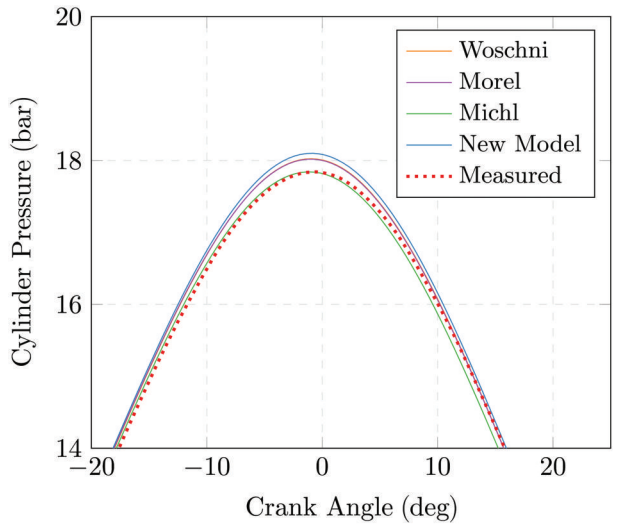

Fig. 5 Example measured versus simulated pressure for a motored case, at a compression ratio of 8.67 and inlet pressure of 0.99 bar for each of the selected models from the literature. Zoomed into the peak at TDC to highlight difference between modeled and measured traces.

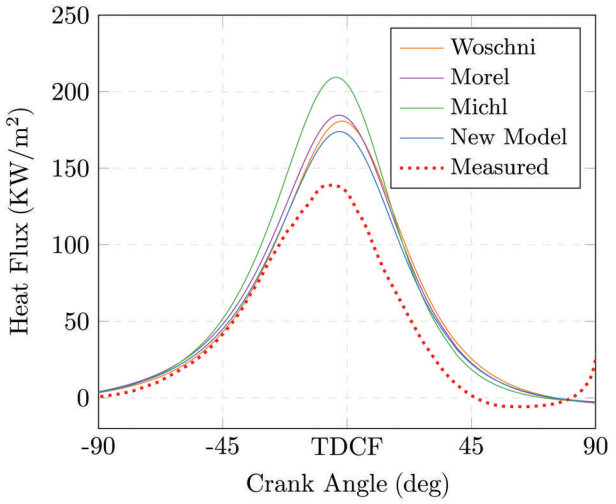

Fig. 6 Measured versus simulated heat flux for the motored case (compression ratio = 8.67, P_{in} = 0.99 bar)

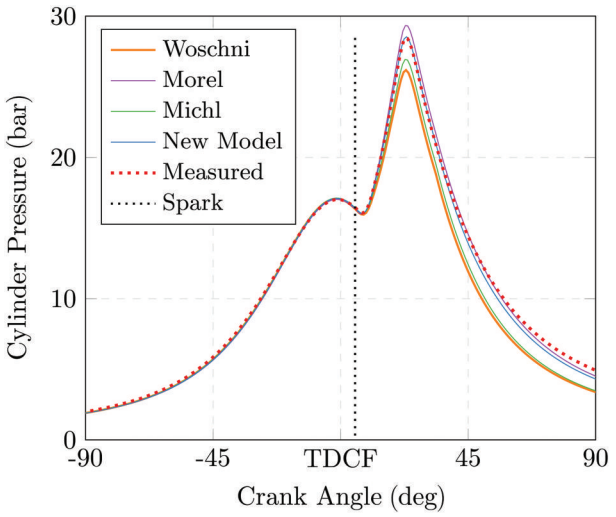

Fig. 7 Measured versus simulated pressure for a representative fired condition (CR = 9, IMEP = 3 bar and lambda = 1.8). Each model was recalibrated to match the compression curve.

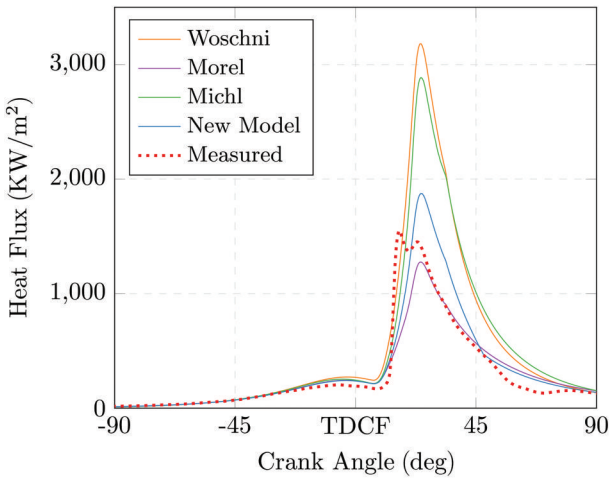

Fig. 8 Measured versus simulated heat flux for a representative fired condition (CR = 9, IMEP = 3 bar and lambda = 1.8)

measurement location does not suffice to represent a spatial average. The measured heat flux for the fired condition in Fig. 8 exhibits two peaks, which likely correspond to the arrival of the flame front at the sensor, and the maximum cylinder temperature. Again, this is not representative of a spatial average, but can be used to derive some insight into the characteristics of heat transfer from hydrogen combustion. The disparity between the measured and simulated heat flux traces during compression may also be indicative of the singular measurement location not being representative of the full chamber spatial average.

The distinctive feature of the measured heat flux in Fig. 8 is its large gradient both during its rise and fall. The latter of these is not well captured by the heat transfer models, which is evident during the expansion stroke in Fig. 7, where the simulated pressure traces fall more rapidly than the measured pressure.

For the example condition shown in Fig. 7, the new model produces a good match during compression and combustion, but still overestimates heat losses during expansion which results in low cylinder pressures in this phase.

Figure 9 compares the normalized root-mean-square error (nRMSE) of the predicted versus measured pressure values during the compression and combustion phase for each model across the entire calibration dataset. For this comparison the compression phase is defined as from 90 CAD BTDC until the ignition angle, and the combustion phase is defined as the period from the ignition angle until 90 CAD ATDC. Both the Morel and New models exhibit a slightly lower spread of error than the Woschni and Michl models during compression, but the median error is very close between all three models. The reduced error during combustion is evident for the Morel and New models, and despite a slightly larger median error for the new model, it exhibits a much lower spread in error for the calibration dataset.

5.2 Validation Dataset. With a wider range of both compression ratio and lambda, the validation dataset provides a sterner test of the heat transfer models. This is reflected in the larger range of error values shown in Fig. 10.

The normalized RMSE for each condition is shown in Fig. 10 for the new model compared to those of Michl [3], Morel [21], and Woschni [15]. Similarly to the process outlined in Sec. 3.3, the heat transfer multiplier was adjusted to match the pressure trace during the compression stroke (before ignition) for each model, with only a single multiplier used for all cases (totalling 26 different combinations of compression ratio and lambda).

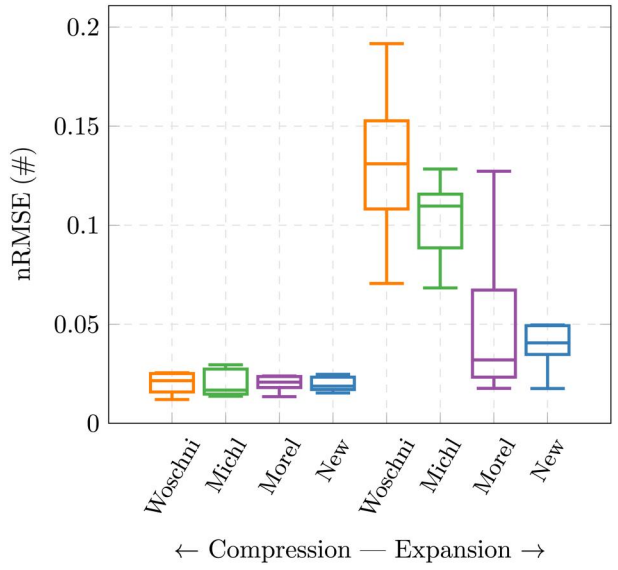

Fig. 9 Box plot comparing the median and spread of the normalized RMSE of pressure from the measured calibration dataset of the compression and combustion phases separately for each heat transfer model. The horizontal lines denote the median, 25th and 75th percentile values.

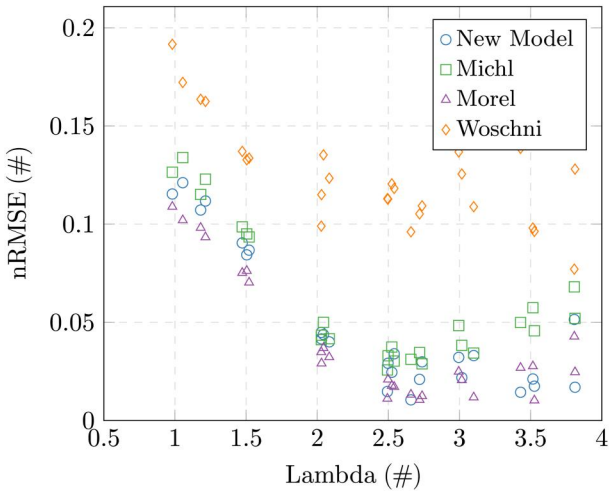

Fig. 10 Normalized RMSE of pressure during the combustion phase for each model when applied to the CFR validation data

All of the models performed satisfactorily during the compression stroke, with one multiplier providing a good match with the precombustion pressure trace for all lambdas and compression ratios. After ignition, however, the Michl model [3] tended to overestimate the heat transfer quite significantly, whereas the Morel model [21], with its lack of combustion term, underestimated the heat transfer during combustion (illustrated in Fig. 7).

Figure 10 reveals similar performance for both the new model and Morel model across all lambda values, with a slightly lower error for the Morel model at conditions close to stoichiometry. An increased deviation during expansion masks the improvement shown by the New model during combustion, which is illustrated in Fig. 7, with Morel's model resulting in a high peak pressure but less error during expansion, and the new model achieving a closer peak pressure but more deviation after combustion is complete. Figure 11 highlights this trait for all the validation cases, showing a consistently high peak pressure (i.e., under-predicted heat transfer) for the Morel model whereas the new model maintains a more accurate prediction of the peak pressure throughout the range of equivalence ratios. Coincidentally, the peak pressure predictions from the Michl model are more accurate than those of the new model for lambda < 2, but this decreases significantly for leaner mixtures.

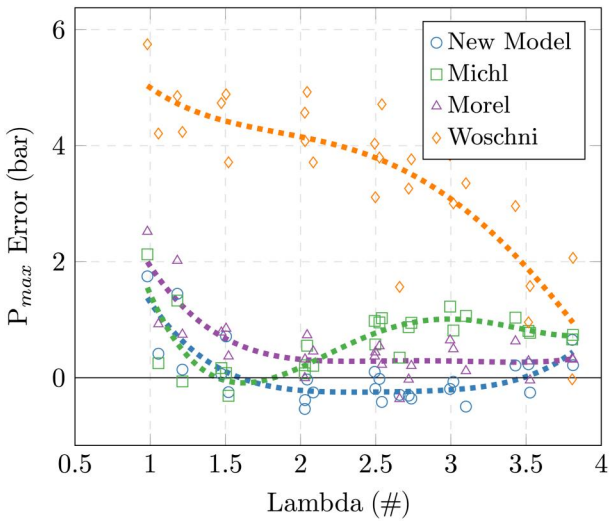

Fig. 11 Error in peak cylinder pressure for each model when applied to the validation data, with polynomial best fit lines demonstrating the trend for each model as lambda varies

6 Conclusion

This study has compared the performance of existing 0D heat transfer correlations on hydrogen combustion in a CFR engine, and derived a new phenomenological heat transfer model that better captures the effect of hydrogen combustion on heat transfer during the compression and combustion phases. This improvement is important for matching the in-cylinder conditions during combustion for a more accurate prediction of combustion rates, emissions and knock. Further development is required to mitigate the over-prediction of heat transfer during the expansion stroke, which will affect predictions of exhaust enthalpy and therefore turbocharger performance.

It has been demonstrated that, for hydrogen combustion, a heat transfer model must take into account the change in mixture properties relative to other fuels, and a well-calibrated turbulence model is required to accurately predict the in-cylinder gas motion, which is critical for heat transfer predictions.

The new model exhibits more consistent performance over a wide range of compression ratios and equivalence ratios without the requirement for recalibration, which is critical for the prediction of heat transfer during the engine development process.

As the data are restricted to only 600 rpm and a low range of loads, validation against data from other engines at higher speeds and loads is still required for this model. Whilst this model shows an improvement against previous heat transfer models for hydrogen combustion, there is scope for further improvement, as shown by the consistent over-prediction of heat losses during expansion.

The omission of tumble effects on the velocity vectors used to calculate the characteristic velocity may impact this model's accuracy for tumble-based combustion systems. Further work is required to account for these effects, either by estimation of the tumble velocity vectors or by adopting the alternative energy field method.

Acknowledgment

The authors would like to thank Sebastian Verhelst and his co-workers at the University of Ghent, and Jamie Turner and his colleagues at KAUST, for sharing their experimental results and details on the engine builds and experimental configurations. This work is supported by the EPSRC Prosperity Partnership project in collaboration with Jaguar Land Rover, the University of Oxford, and Siemens Digital Industries Software under project EP/T005327/1 "Centre of Excellence for Hybrid Thermal Propulsion Systems".

Funding Data

- Engineering and Physical Sciences Research Council (Award No. EP/T005327/1; Funder ID: 10.13039/501100000266).

Data Availability Statement

The datasets generated and supporting the findings of this article are obtainable from the corresponding author upon reasonable request.

Nomenclature

Roman Letters

k = turbulent kinetic energy ($m^2\ s^{-2}$)
K = mean kinetic energy ($m^2\ s^{-2}$)
ε = turbulence dissipation rate ($m^2\ s^{-3}$)
$\mathbf{q}$ = heat flux vector ($W\ m^{-2}$)
h = convective heat transfer coefficient ($W\ m^{-2}\ K^{-1}$)
L_c = characterisitc length (m)
v_c = characteristic velocity ($m\ s^{-2}$)
C_p = specific heat capacity ($J\ kg^{-1}\ K^{-1}$)
C_f = friction coefficient
V = volume (m^3)
H_c = instantaneous cylinder height (m)
B = cylinder bore (m)
U = mean gas velocity ($m\ s^{-1}$)
u' = turbulent intensity ($m\ s^{-1}$)
U_p = instantaneous piston speed ($m\ s^{-1}$)
$\bar{S}_p$ = mean piston speed ($m\ s^{-1}$)
P_{in} = inlet pressure (bar)
nRMSE = normalized root mean square error

Greek Symbols

α = thermal diffusivity ($m^2\ s^{-1}$)
μ = dynamic viscosity ($m^2\ s^{-1}$)
ρ = density ($kg\ m^{-3}$)
κ = thermal conductivity ($W\ m^{-1}\ K^{-1}$)
Ω = fluid properties term
Ξ = combustion term

Dimensionless Groups

Pr = Prandtl number
Nu = Nusselt number
Re = Reynolds number
St = Stanton number

Subscripts

b = burned zone
u = unburned zone
w = wall

Appendix A: Turbulence Equations

$$E_{in} = (1 - C_T)\frac{1}{2}\dot{m}_{in}v_{in}^2 \tag{A1}$$

$$P_k = C_\beta \nu_T \frac{2mK}{L_g^2} - \frac{2}{3}mk\left(\frac{\dot{\rho}}{\rho}\right) - \frac{2}{3}m\nu_T\left(\frac{\dot{\rho}}{\rho}\right)^2 \tag{A2}$$

$$P_\varepsilon = \frac{\varepsilon}{k}\left[5.76C_\beta \nu_T \frac{mK}{L_g^2} - 2mk\left(\frac{\dot{\rho}}{\rho}\right) - \frac{2.64}{3}m\nu_T\left(\frac{\dot{\rho}}{\rho}\right)^2\right] \tag{A3}$$

where $\nu_T = C_\mu k^2/\varepsilon$ is the turbulent viscosity ($C_\mu = 0.09$ is a standard k–ε model constant).

Appendix B: Viscosity and Conductivity Correlation Performance

Figures for Viscosity and Conductivity correlation comparisons between derived relationships and those published by Michl et al. [3].

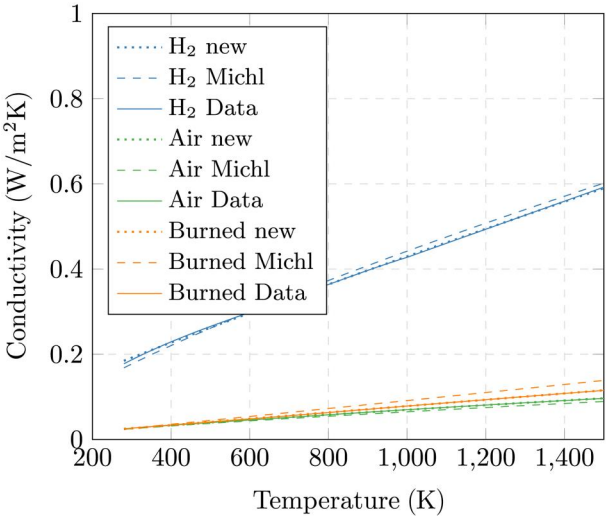

Fig. 12 Conductivity results for both Michl et al.'s correlation and the new correlation compared to the calculated results using the mechanism from Sun et al. [37]

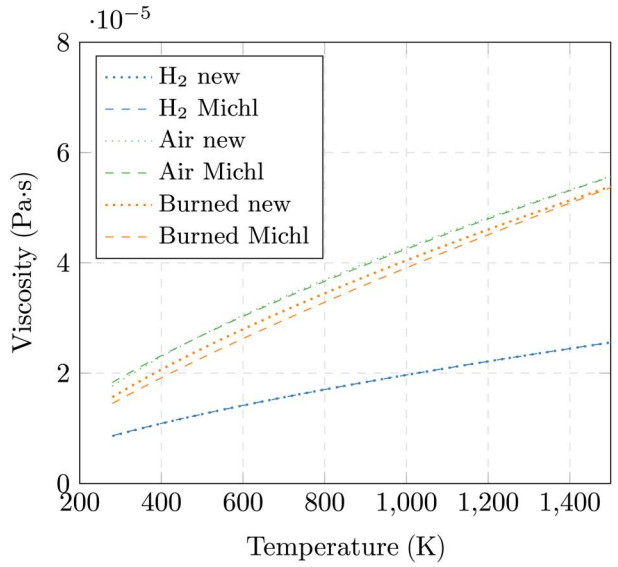

Fig. 13 Viscosity results for both Michl et al.'s correlation and the new correlation compared to the calculated results using the mechanism from Sun et al. [37]

References

[1] Frasci, E., Cervone, D., Nacci, G., Sementa, P., Arsie, I., Jannelli, E., and Vaglieco, B. M., 2023, "Energy and Pollutants Analysis of a Series HEV Equipped With a Hydrogen-Fueled SI Engine," SAE Paper No. 2023-24-0132.

[2] Official Journal of the European Union, 2023, "Regulation (EU) 2023/851 of the European Parliament and of the Council of 19 April 2023 Amending Regulation (EU) 2019/63 As Regards Strengthening the CO_2 Emission Performance Standards for New Passenger Cars and New Light Commercial Vehicles in Line With the Union's Increased Climate Ambition," Official Journal of the European Union, Luxembourg, No. OJ L110/5.

[3] Michl, J., Neumann, J., Rottengruber, H., and Wensing, M., 2016, "Derivation and Validation of a Heat Transfer Model in a Hydrogen Combustion Engine," Appl. Therm. Eng., **98**, pp. 502–512.

[4] Shudo, T., Nabetani, S., and Nakajima, Y., 2001, "Analysis of the Degree of Constant Volume and Cooling Loss in a SI Engine Fuelled With Hydrogen," Int. J. Engine Res., **2**(1), pp. 81–92.

[5] Shudo, T., and Suzuki, H., 2002, "Applicability of Heat Transfer Equations to Hydrogen Combustion," JSAE Rev., **23**(3), 303–308.

[6] Nefischer, A., Hallmannsegger, M., Wimmer, A., and Pirker, G., 2009, "Application of a Flow Field Based Heat Transfer Model to Hydrogen Internal Combustion Engines," SAE Paper No. 2009-01-1423.

[7] Borman, G., and Nishiwaki, K., 1987, "Internal Combustion Engine Heat Transfer," Prog. Energy Combust. Sci., **13**(1), pp. 1–46.

[8] Broekaert, S., De Cuyper, T., Chana, K., De Paepe, M., and Verhelst, S., 2015, "Assessment of Empirical Heat Transfer Models for a CFR Engine Operated in HCCI Mode," SAE Paper No. 2015-01-1750.

[9] Broekaert, S., De Cuyper, T., De Paepe, M., and Verhelst, S., 2017, "Evaluation of Empirical Heat Transfer Models for HCCI Combustion in a CFR Engine," Appl. Energy, **205**, pp. 1141–1150.

[10] Hensel, S., Sarikoc, F., Schumann, F., Kubach, H., and Spicher, U., 2009, *Investigations on the Heat Transfer in HCCI Gasoline Engines*, SAE Paper No. 2009-01-1804.

[11] Lounici, M. S., Loubar, K., Balistrou, M., and Tazerout, M., 2011, "Investigation on Heat Transfer Evaluation for a More Efficient Two-Zone Combustion Model in the Case of Natural Gas SI Engines," Appl. Therm. Eng., **31**(2–3), pp. 319–328.

[12] Broekaert, S., Demuynck, J., De Cuyper, T., De Paepe, M., and Verhelst, S., 2016, "Heat Transfer in Premixed Spark Ignition Engines Part I: Identification of the Factors Influencing Heat Transfer," Energy, **116**, pp. 380–391.

[13] Verhelst, S., and Wallner, T., 2009, "Hydrogen-Fueled Internal Combustion Engines," Prog. Energy Combust. Sci., **35**(6), pp. 490–527.

[14] Soloiu, V., Gaubert, R., Moncada, J., Wiley, J., Williams, J., Harp, S., Ilie, M., Molina, G., and Mothershed, D., 2019, "Reactivity Controlled Compression Ignition and Low Temperature Combustion of Fischer-Tropsch Fuel Blended With N-Butanol," Renewable Energy, **134**, pp. 1173–1189.

[15] Woschni, G., 1967, "A Universally Applicable Equation for the Instantaneous Heat Transfer Coefficient in the Internal Combustion Engine," SAE Paper No. 670931.

[16] Gamma Technologies, 2022, "GT Power Engine Performance Manual (Version 2022)," Gamma Technologies, Westmont, IL.

[17] Shudo, T., and Suzuki, H., 2002, "New Heat Transfer Equation Applicable to Hydrogen-Fuelled Engines," ASME Paper No. ICEF2002-515.

[18] Chang, J., Guralp, O., Filipi, Z., Assanis, D., Kuo, T.-W., Najt, P., and Rask, R., 2004, "New Heat Transfer Correlation for an HCCI Engine Derived From Measurements of Instantaneous Surface Heat Flux," SAE Paper No. 2004-01-2996.

[19] Olmeda, P., Martín, J., Novella, R., and Carreño, R., 2015, "An Adapted Heat Transfer Model for Engines With Tumble Motion," Appl. Energy, **158**, pp. 190–202.

[20] Choi, W., and Song, H. H., 2020, "Composition-Considered Woschni Heat Transfer Correlation: Findings From the Analysis of Over-Expected Engine Heat Losses in a Solid Oxide Fuel Cell-Internal Combustion Engine Hybrid System," Energy, **203**, p. 117851.

[21] Morel, T., and Keribar, R., 1985, "A Model for Predicting Spatially and Time Resolved Convective Heat Transfer in Bowl-in-Piston Combustion Chambers," SAE Paper No. 850204.

[22] Schubert, C., Wimmer, A., and Chmela, F., 2005, "Advanced Heat Transfer Model for CI Engines," SAE Paper No. 2005-01-0695.

[23] Merker, G., Schwarz, C., and Teichmann, R., 2012, *Combustion Engines Development: Mixure Formation, Combustion, Emissions and Simulation*, Springer Science and Business Media, Berlin.

[24] Irimescu, A., Merola, S. S., Tornatore, C., and Valentino, G., 2015, "Development of a Semi-Empirical Convective Heat Transfer Correlation Based on Thermodynamic and Optical Measurements in a Spark Ignition Engine," Appl. Energy, **157**, pp. 777–788.

[25] Hohenberg, G., 1979, "Advanced Approaches for Heat Transfer Calculations," SAE Paper No. 790825.

[26] Morel, T., Rackmil, C. I., Keribar, R., and Jennings, M. J., "Model for Heat Transfer and Combustion in Spark Ignited Engines and Its Comparison With Experiments," SAE Paper No. 880198.

[27] Huber, K., Woschni, G., and Zeilinger, K., 1990, Investigations on Heat Transfer in Internal Combustion Engines Under Low Load and Motoring Conditions, SAE Paper No. 905018.

[28] Demuynck, J., 2012, "A Fuel Independent Heat Transfer Correlation for Premixed Spark Ignition Engines," Ph.D. thesis, Ghent University, Ghent, Belgium.

[29] De Cuyper, T., Demuynck, J., Broekaert, S., De Paepe, M., and Verhelst, S., 2016, "Heat Transfer in Premixed Spark Ignition Engines Part II: Systematic Analysis of the Heat Transfer Phenomena," Energy, **116**, pp. 851–860.

[30] Demuynck, J., Chana, K., De Paepe, M., and Verhelst, S., 2013, "Evaluation of a Flow-Field-Based Heat Transfer Model for Premixed Spark-Ignition Engines on Hydrogen," SAE Paper No. 2013-01-0225.

[31] Fogla, N., Bybee, M., Mirzaeian, M., Millo, F., and Wahiduzzaman, S., 2017, "Development of a K-k-ε Phenomenological Model to Predict in-Cylinder Turbulence," SAE Int. J. Engines, **10**(2), pp. 562–575.

[32] Bozza, F., Teodosio, L., De Bellis, V., Fontanesi, S., and Iorio, A., 2019, "A Refined 0D Turbulence Model to Predict Tumble Turbulence in SI Engines," SAE Paper No. 03-12-01-0002.

[33] Bozza, F., Teodosio, L., De Bellis, V., Fontanesi, S., and Iorio, A., 2018, "Refinement of a 0D Turbulence Model to Predict Tumble and Turbulent Intensity in SI Engines. Part II: Model Concept, Validation and Discussion," SAE Paper No. 2018-01-0856.

[34] Hall, M. J., and Bracco, F. V., 1987, "A Study of Velocities and Turbulence Intensities Measured in Firing and Motored Engines," SAE Paper No. 870453.

[35] Demuynck, J., Raes, N., Zuliani, M., De Paepe, M., Sierens, R., and Verhelst, S., 2009, "Local Heat Flux Measurements in a Hydrogen and Methane Spark Ignition Engine With a Thermopile Sensor," Int. J. Hydrogen Energy, **34**(24), pp. 9857–9868.

[36] Nguyen, D., Kar, T., and Turner, J. W. G., 2023, "Performance, Emissions, and Combustion Characteristics of a Hydrogen-Fueled Spark-Ignited Engine at Different Compression Ratios: Experimental and Numerical Investigation," Energies, **16**(15), p. 5730.

[37] Sun, W., Zhao, Q., Curran, H. J., Deng, F., Zhao, N., Zheng, H., Kang, S., et al., 2022, "Further Insights Into the Core Mechanism of H_2/Co/NOx Reaction System," Combust. Flame, **245**, p. 112308.